INVESTIGATION ON ELECTROCHEMICAL CORROSION BEHAVIOR OF EUTECTIC Al-Si AUTOMOTIVE ALLOY IN 0.2 M HCl, 0.2 M NaOH, AND 0.2 M NaCl ENVIRONMENTS

Mohammad Salim Kaiser[1], Akib Abdullah Khan[2], Somlata Dev Sharma[2], Maglub Al Nur[2]

[1]*Directorate of Advisory, Extension, and Research Services*
Bangladesh University of Engineering and Technology
Dhaka-1000, Bangladesh
[2]*Department of Mechanical Engineering*
Bangladesh University of Engineering and Technology
Dhaka-1000, Bangladesh
E-mail: mskaiser@iat.buet.ac.bd

Received 02 September 2022
Accepted 26 October 2022

ABSTRACT

This study aimed to evaluate the electrochemical corrosion behavior at the eutectic level of Al-Si automotive alloy in 0.2 M HCl, 0.2M NaCl, and 0.2M NaOH solutions at room temperature. By EIS method in accordance with the specific equivalent circuits of the system, and also by recording Tafel dependences, data were obtained on the kinetic and corrosion parameters in the studied environments for two types of alloys - Al-Si alloy with a eutectic composition of Si (12.7 wt. %) and Al-Si alloy containing traces of silicon (0.2 wt. %). Both the EIS data and the Tafel plots disclosed to addition of Si improved the corrosion resistance in the Al-Si alloy in NaCl and HCl environments. In contrast, the opposite phenomenon was observed in the NaOH environment. Added Si improved corrosion resistance by forming MgO and SiO_2 layers; nevertheless, OH^- more aggressively attacks the surface than Cl^- ions, hindering the corrosion-resisting mechanism by Si. The alloys showed the best corrosion resistance in NaCl solution. In contrast, NaOH was the most destructive, followed by HCl solution, as a more compact and uniform film was formed in NaCl solution. The open circuit potential enthused to the nobler direction in eutectic alloys in NaCl and HCl solution, while NaCl showed comparatively higher open circuit potentials (OCP) than HCl and NaOH. The corrosion current from Tafel analysis and the polarization resistance from EIS analysis showed the maximum values in NaCl solution and the minimum in NaOH solution, as the corrosive attack by OH^- was more damaging. The optical and SEM images revealed that scratch marks on polished surfaces were disappeared, and protective layers are formed after corrosion, which are thicker and more compact in the NaCl environment and in higher Si added alloy under NaCl and HCl solution, NaOH being an exception. These images depicted maximum damage in NaOH solution, and then in HCl solution, NaCl showed the minimum damage.

Keywords: Eutectic Al-Si alloy, corrosion, EIS, Tafel plots, Bode and Nyquist coordinates.

INTRODUCTION

Aluminum-based alloys with Si as the primary alloying element are progressively used in a wide range of lightweight components in transportation and construction due to their excellent properties [1 - 3]. Because of its extreme purity, high electrical conductivity, strength, and high technical value, corrosion of Al alloys have been the focus of numerous investigations [4]. Most useful metals, fortunately, react with the environment to generate protective coatings of oxide, which keep the metals from entering the solution as ions. These protective layers are thin and reproducible and form after mechanical polishing. However, when immersed in a solution, these layers thicken rapidly, making the oxide thicker than the layer formed in the air [5]. This oxide film remains stable in an aqueous solution but is dissolved quickly in the 4.0 to 8.5 pH range. Beyond

this range, the film re-forms after damage [6 - 8]. HCl, NaOH and NaCl can contact the surfaces of an engine cylinder or piston. Hydrochloric acid is produced when the combustion of a liquid phase mixture containing a hydrocarbon occurs in a diesel engine [9]. Acids are produced from the decomposition of biodiesel [10 - 12] and are also produced by the oxidation of petroleum diesel [13 - 15]. In most fuel refineries, sodium hydroxide is used as a reagent [16 - 18]. NaOH and NaCl can mixed with the engine fuel as Na carriers [19]. Again, through salt driers in refineries, tankers which get in contact with seawater while flushing *etc.*, NaCl can leach into the fuel [18]. Also, engine radiators are often refilled with locally available water that contains NaCl. In marine applications, the engine parts made with Al-Si alloy contact seawater which also contains NaCl. Various elements such as Si, Cu, Ni, Fe, Mn, etc. are added as alloying elements in the alloy matrix to upgrade various mechanical and physical properties of aluminum alloys [20]. Silicon as an alloying element improves not only strength but surface quality, corrosion resistance, hardness and other properties in the alloy [21, 22]. The eutectic system of Al-Si has two solid phases, of which the eutectic composition is 12.2 ± 0.1 wt. % Si [23]. The electrochemical impedance spectroscopy methods are the most powerful steady-state methods in electrochemistry, estimating a number of parameters of analogous electrochemical systems like capacitance, resistance, electrolyte-passive film *etc.* [24]. In EIS, actual electrochemical processes taking place in the material are related to the theoretical circuit elements by fitting alternating voltage and frequency data with analogous electrical circuits. In EIS, an electronic device is subjected to an AC potential, the response of the AC current is measured, and changes in phase shift and amplitude are recorded throughout a range of frequencies. By inspecting the current response across different frequencies it is possible to separate operations occurring on different timescales, making it a suitable tool for distinguishing electronic and ionic processes in mixed conductors [25]. The potentiodynamic polarization test (Recording of Tafel plots) is one of the most frequently used techniques for assessing specimen corrosion. The active/passive corrosion rates of different potentials can be accurately determined using this method, which also helps in understanding the various processes taking place on the surface of metal samples [26].

Although Al-Si alloys exhibit outstanding both physical and mechanical properties, but the corrosion resistance of these alloys in aggressive environments is not vastly studied. Recently, some studies are going on evaluating the corrosion resistance of these alloys in different media [27, 28]. Again, the role of Si on electrochemical corrosion performance in NaCl solution has been studied previously [22]. Therefore, the objective of this exercise is to understand the corrosion nature of Al-Si alloy with eutectic composition of Si (12.7 wt. %) compared to an alloy without Si, keeping the amount of other constituting alloying elements constant in HCl, NaOH and NaCl solution of 0.2 M concentration.

EXPERIMENTAL

Materials

Available in the market, aluminium, copper, magnesium, and Al-50 wt. % Si master alloy ingots of pure quality were employed for this purpose. To evaluate the effect of Si alone as an alloying element, a sample with eutectic composition is taken and another without Si, keeping levels of Cu and Mg constant. Although it was supposed to prepare a sample without Si, some small amount of Si was intruded into the alloy. Fe, Ni, Sn, and Sb were also detected as trace impurities in the alloys. The following are the primary ingredients of the two alloys (in wt. %):

Alloy 1: Al - 0.2 % Si - 2.2 % Cu - 0.8 % Mg, presented below as “trace Si added alloy”, 0.2Si;

Alloy 2: Al - 12.7 % Si - 2.2 % Cu - 0.8 % Mg, presented below as “eutectic Si added alloy”, 12.7Si.

These alloys were melted in a graphite crucible using a natural gas pit furnace. An appropriate flux cover was employed to prevent oxidation during the melting process. Preheating a 20 × 200 × 300 mm^3 sized mold of mild steel to 250°C was necessary for the casting. For homogenization, a muffle furnace was utilized, heated at 450°C for 12 hours and air-cooled to allow the stresses relieving. After homogenizing the samples, were solutionized for two hours at 535°C and then quenched in salt water until they reached a single phase super saturated zone. The chemical composition of the test alloys was determined using a Shimadzu PDA 700 optical emission spectrometer. The natural oxide layer was then machined away from the alloys. Machining was

done to produce rectangular samples (5 mm × 5 mm x 12 mm) from the cast products. The samples were aged at 200°C for 4 hours for achieving peak strength [29]. The sample surfaces except the 5 mm × 5 mm surface were coated with PVC heat shrinkable tube so that other surfaces remain unaffected. The exposed surfaces were polished with 320, 600, 800, 1200, and 2000 grit emery sheets to achieve a smooth and refined surface. The whole experiment was performed at 25 ± 1 °C.

Electrochemical Impedance Spectroscopy (EIS) Technique

A computerized CH Instruments - Electrochemical Workstation, connected to a three-electrode system of 100 mL capacity, was used to perform the EIS technique on the experimental alloys. The 0.2 M NaCl, HCl, and NaOH electrochemical cells are prepared by the solutions of the corresponding electrolytes mixed with deionized water. As reference electrode, Ag/AgCl electrode, as a counter electrode, a platinum rod, and as the working electrode the experimental samples were used. Only 5 × 5 millimeters of each working electrode surface was exposed to the corresponding solution. The working electrode was connected to the working station by crocodile clips. The working electrode was dipped in the concerned solution to prepare the polarization cells. The system was given a time interval of about half an hour to achieve a steady state. A frequency domain from 0.2 Hz to 100 kHz was chosen and the excitation AC signal had an amplitude of 5 mV peak to peak, prior to establishing the open circuit potential (OCP). To ensure more precision, the solutions were refilled occasionally throughout the experimental runs. After concluding the experiment at open circuit potential, analogous circuits were created using the tool EC-Lab Analyst. The response values were matched to the analogous circuits with the greatest precision achievable which are presented in Fig. 1. The Randle's circuit is used to model the electrochemical systems of NaCl and HCl media (Fig. 1(a)), and another circuit was used for NaOH medium which was previously used to model electrochemical system of Al alloy in NaOH environment [30]. Fig. 1(a) consists of the circuit components solution resistance (R_s), polarization resistance or corrosion resistance (R_p), and effective double layer capacitance ($C_{p(eff)}$), and Fig. 1(b) consists of the solution resistance (R_s), an inductive element L, two R_1-C_1 and R_2-C_2 terms in series with L.

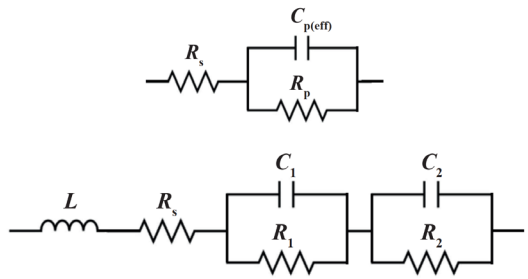

Fig. 1. The equivalent circuit for fitting impedance data of the Al-based alloys in solutions of a - 0.2 M NaCl and 0.2 M HCl, b - 0.2 M NaOH.

Potentiodynamic Polarization Technique

The tests on potentiodynamic polarization were performed using the same experimental setup as the EIS analysis. The potential sweep was carried out from -1 V to +1 V against the reference electrode. A scan rate of 0.50 mV s^{-1} was selected. As a result, the configuration was able to generate a steady state open circuit potential. The required Tafel plot was created following the conclusion of the experiment. The Tafel polarization plot was used to measure the corrosion potential (E_{corr}) in millivolts, the corrosion current (I_{corr}) in micro amps, and the corrosion rate in mm $year^{-1}$ for each of the experimental alloys. The established formula aaccording to ASTM standard G102 is:

$$\text{Corrosion rate} = \frac{I_{corr}\, K\, EW}{\rho\, A} \quad (1)$$

where I_{corr} is the corrosion current in amperes, K is the constant which defines the units of corrosion rate in mm $year^{-1}$, EW and ρ are the equivalent weight and density of the alloys respectively and A is the area exposed to the surrounding environment.

The sample surfaces appeared to have degraded after the experiment, and they were examined with a standard optical microscope and a scanning electron microscope.

RESULTS AND DISCUSSION

Impedance Measurement

The Nyquist plots of the traced Si along with 12.7Si added alloys are shown in Fig. 2 for salt, acidic and basic media, respectively. The semicircle like capacitive-resistive model is used to derive the real Z_{real} and imaginary Z_{imag} component of the impedances. The corrosion of aluminium-silicon alloy is regulated by

a charge transfer process, as evidenced by a separate complete semicircular appearance on the Nyquist diagrams [31]. Frequency dispersion may cause some distortion in the diagrams [32]. The shape of a Nyquist plot depends on the electrode matrix, like the working electrode composition *etc.* and the electrochemical responses at the surface of the working electrode or in the bulk station [33]. Fig. 2 displays depressed Nyquist plots, suggesting that they are not ideal semicircles as predicted by EIS theory. The non-ideal behavior of the double layer as a capacitor explains this disparity [34, 35]. The range of the values of Z_{real} is the highest for NaCl solution, HCl having a medium range, whereas, the NaOH solution has a short range of values. This indicates the maximum corrosion resistance in NaCl solution, followed by HCl and NaOH solution. Again, the maximum value of Z_{real} is higher for 12.7Si added alloy than 0.2Si added alloy in case of NaCl and HCl solution, and the opposite phenomenon is observed in case of NaOH solution. The values of Z_{real} are lower in HCl from NaCl environment. So, Fig. 2(b) is prepared with a lower scale. Again, the real values of impedance under NaOH environment are even lower than those under HCl environment. Eventually, the Nyquist diagram (Fig. 2(c)) is plotted with even lower scale.

The computerized CH instruments - Electrochemical Workstation generated the EIS data for the experimental alloys, which were then simulated by EC-lab Analyst. The best fitted circuit models are shown in Fig. 1 and the data generated from the fitted circuit is presented in Table 1 and Table 2. Table 1 shows the polarization resistance (R_p), solution resistance (R_s) and the effective electrical double layer capacitance ($C_{p(eff)}$) are represented for 0.2 M NaCl and 0.2 M HCl solution. Extremely low values of R_s are observed compared to R_p. Table 2 shows the corresponding circuit components of the impedance data in case of 0.2 M NaOH solution. The sum of R_1 and R_2 might represent the polarization resistance R_p [30]. The values of R_s are connected to the solution used and those of R_p are linked to the working electrodes. The polarization resistance informs about the reactivity rate of the surface with the environment. R_p is inversely proportional to the material corrosion rate [32, 36 - 38]. The data suggest highest R_p values for NaCl solution and for HCl and NaOH chronologically. Additionally, 12.7Si added alloys show higher R_p for both NaCl and HCl solutions. Whereas it appears that 0.2Si added alloy

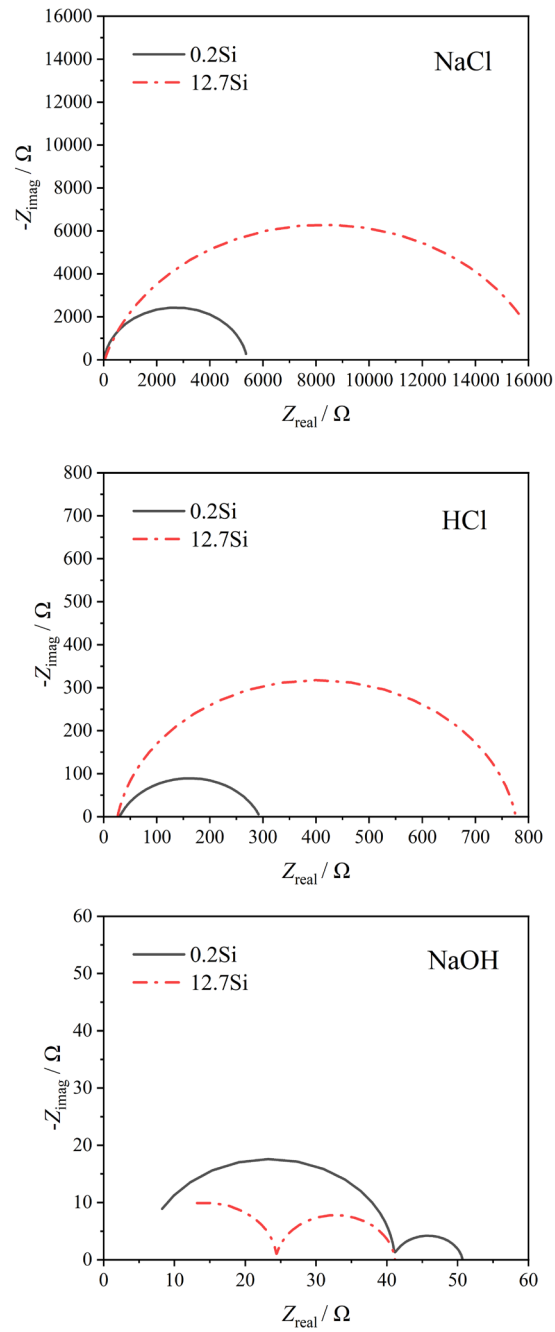

Fig. 2. Nyquist diagrams of the eutectic and trace Si added alloys in environment of a) - 0.2 M NaCl, b) - 0.2M HCl, c) - 0.2M NaOH.

has higher value of R_p compared to 12.7Si in NaOH solution. The added Si provides a corrosion inhibition by forming Mg_2Si intermetallic particles, which eventually transform into MgO and SiO_2 layers, protecting the alloy surface from corrosion. However, eutectic Si at the alloy grain boundaries acts as cathodic clusters for

galvanic corrosion [39]. Although MgO and SiO_2 can protect the alloy surface from corrosion in NaCl and HCl environment, they fail to do so in NaOH environment as the aggressive OH^- thins out the protective oxide layers and attack the grain boundaries. Hence, the effect of Si is rather deleterious in NaOH environment. It is concluded that NaCl shows the best corrosion performance followed by HCl and NaOH, where in both NaCl and HCl the eutectic alloy has better corrosion resistance, NaOH showing the opposite phenomena. Cl^- dissolved in the solution attacks the alloy surface and results in pitting corrosion, where the corrosion is more destructive in HCl media as the solubility of Al_2O_3 is enhanced in alkaline and acid media [40, 41]. Besides, HCl induces rapid corrosion of Al [5]. Al corrosion is more severe in NaOH solution than HCl and NaCl due to the relentless attack by the OH^- corrosive agents, which has high adsorption at little distances.

Aqueous sodium hydroxide dissolves the aluminium oxide layer:

$$Al_2O_3(s) + 2NaOH(aq) \rightarrow 2NaAlO_2(aq) + H_2O(l) \quad (2)$$

$$2Al(s) + 2NaOH(aq) + 2H_2O(l) \rightarrow 2NaAlO_2(aq) + 3H_2(g) \quad (3)$$

HCl provides an inherent cathodic defense from anion-metal interactions which NaOH does not [42]. In case of HCl and NaCl environment, higher corrosion resistance is found in higher silicon added alloy as Si forms Mg_2Si intermetallic phase with Mg, which is anodic to the aluminium matrix and may enhance the corrosion resistance of the alloys to some extent. The Mg_2Si precipitations form SiO_2 and MgO [22, 43, 44]. However, in NaOH there is higher rate of H_2 generation on the exposed surfaces of the alloy with eutectic amount of Si, which may be responsible for the increased corrosion [39].

The increase in Si concentration has a detrimental effect on the corrosion resistance in Al-Si alloys according to previous studies [45]. Moreover, superfluous amount of Si rises the cathodic rate of reaction, as Si tends to gather along the grain boundary, leading to inter-granular corrosion and stress-corrosion cracks [46]. It can be decided from the EIS test results that the detrimental effects of Si on corrosion are counter-balanced by the positive of Mg_2Si intermetallic in case of both 0.2 M HCl and NaCl environment. Previous research has shown that as corrosion resistance rises, the value of open circuit potential shifts toward nobler (positive) direction [36]. The open circuit potential of 12.7Si added alloy is more positive than of 0.2Si added alloy in NaCl and HCl environment, which aligns with the previous research, and the OCP value decreases in higher Si added alloy in NaOH environment, which lies with our previous observation, too.

The impedance data obtained are shown as Bode plots in Fig. 3. The absolute values of impedance and frequencies are plotted on the Bode magnitude plot (Figs. 3(a), 3(b), 3(c)) and the phase angles and frequencies are plotted on the Bode phase plot (Figs. 3(a*), 3(b*), 3(c*)). $Z_{modulus}$ and θ are defined as,

$$\theta = \tan^{-1}\frac{-Z_{imaginary}}{Z_{real}} \quad (4)$$

$$Z_{modulus} = \sqrt{Z_{real}^{\ 2} + Z_{imaginary}^{\ 2}} \quad (5)$$

Table 1. Electrochemical impedance spectroscopy experimental results for 0.2 M NaCl and HCl solution.

Environment	Alloy	R_s (Ω)	R_p (Ω)	C_p (μF)	OCP (V/SCE)	Goodness of Fit
NaCl	0.2Si	20.17	5381	7.16	-0.68407	0.003151
	12.7Si	38.39	16514	6.803	-0.67207	0.003361
HCl	0.2Si	29.98	264	71.5	-0.89805	0.03338
	12.7Si	26.03	750	10.81	-0.68843	0.02856

Table 2. Electrochemical impedance spectroscopy experimental results for 0.2 M NaOH solution.

Environment	Alloy	R_s (Ω)	R_1 (Ω)	R_2 (Ω)	C_1 (μF)	C_2 (μF)	L (μH)	OCP (V/SCE)	Goodness of Fit
NaOH	0.2Si	4.994	36	9.691	0.1407	519	2.266	-1.3742	0.1943
	12.7Si	4.092	16.76	20.27	150	0.0874	0.297	-1.3832	0.02533

In Figs. 3(a), 3(b), and 3(c) it is observable that |*Z*| is higher at low frequency in HCl than NaOH, also in NaCl than HCl, depicting that the corrosion resistance is maximum in NaCl and minimum in NaOH environment. Again, |*Z*| is higher at close to zero frequency in 12.7 wt. % Si added alloy in sodium chloride and hydrochloric acid solutions. On the contrary, |*Z*| is higher in 0.2 wt. % Si added alloy at close to zero frequency in NaOH environment. These results align with those from Nyquist diagrams. In Figs. 3(a*), 3(b*), and 3(c*) it is seen that there is no phase shift at very low and very high frequencies, showing resistive response, and at medium frequencies the phase shift is closer to -90°, which denote capacitive response.

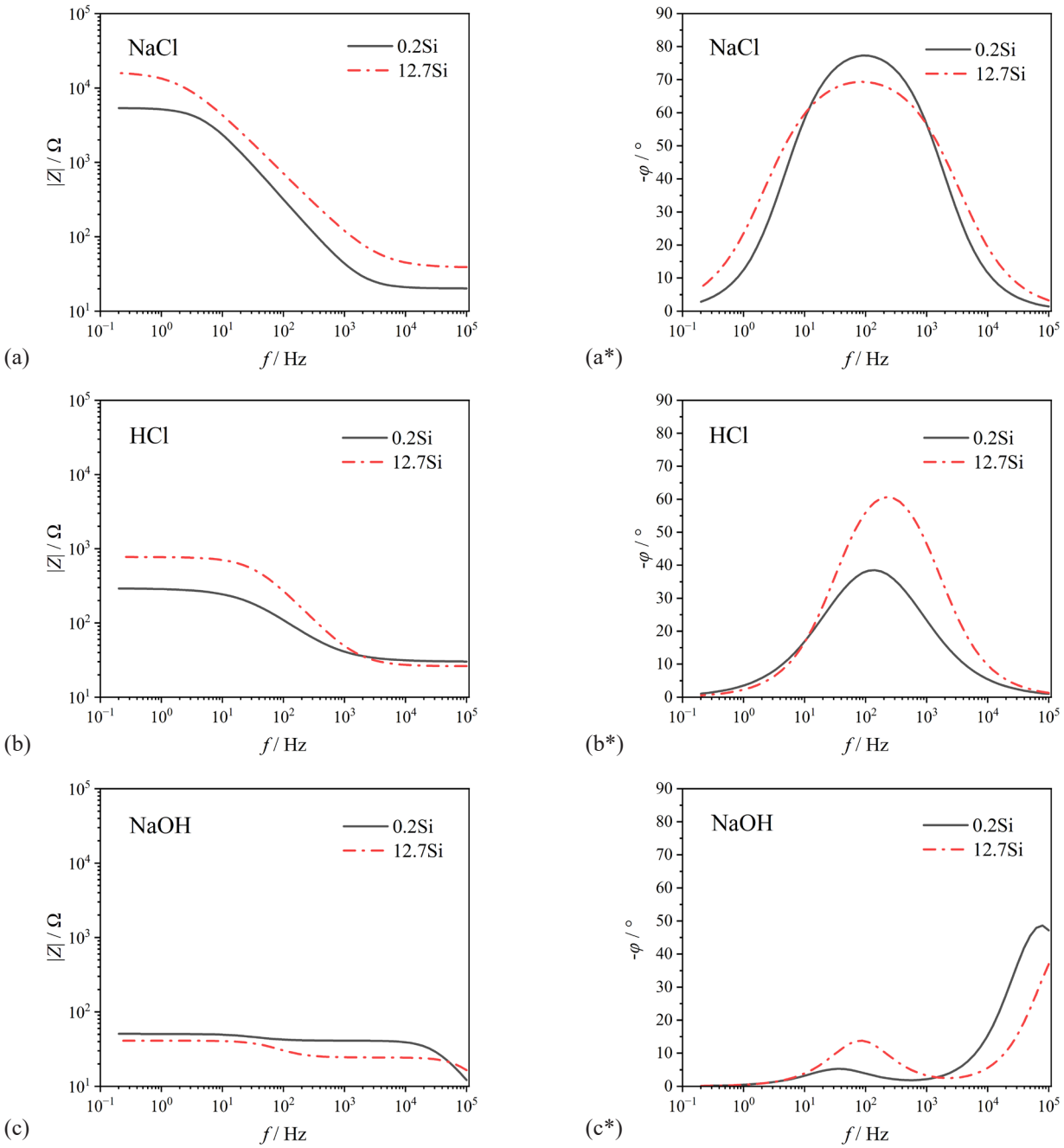

Fig. 3. Bode magnitude (a-c) and phase plots (a*-c*) for trace Si (curves 1) and 12.7Si (curves 2) added Al-Si alloys in environment of 0.2 M: a, a* - NaCl, b, b* - HCl and c, c* - NaOH.

Potentiodynamic Polarization Analysis

Table 3 represents the results the corrosion current (I_{corr}), corrosion potential (E_{corr}) and the corrosion rate or the loss in mm Year^{-1} obtained from potentiodynamic polarization analysis.

Although in both HCl and NaCl environments the corrosion rate decreases as wt. % of Si is increased, in caustic soda environment the opposite trend is observed, which is like the result found in EIS analysis. According to previous research, a further positive value of corrosion potential dictates upgraded corrosion resistance [47]. Investigating our results, more positive values of E_{corr} are found for NaCl environment compared to the HCl and NaOH environments. Like the previous results, more positive values of corrosion potential are found in 12.7Si added alloy in HCl and NaCl corrosive environment showing better corrosion resistance in alloy with higher amount of Si, while NaOH being an exception. Surface characteristics like surface porosity, the presence of unmolten powder, and melt pool border density on the surface could all contribute to slight scatter in the potentiodynamic curves [48]. Another observation is, the corrosion rate is considerably higher in NaOH compared to both HCl and NaCl solutions. Earlier investigations also found equivalent results. Hydrochloric acid shows less corrosion tendency than sodium hydroxide due to underlying cathodic protection arisen from anion-metal interactions [42]. The sodium chloride environment shows the best corrosion performance among all environments in consideration, since the breakdown and pitting corrosion by Cl^- ions are more pronounced in lower pH values [5].

Fig. 4 shows the Tafel plots for the experimental trace Si added alloy and 12.7Si added alloy in 0.2 M NaCl, 0.2 M HCl and 0.2 M NaOH environments.

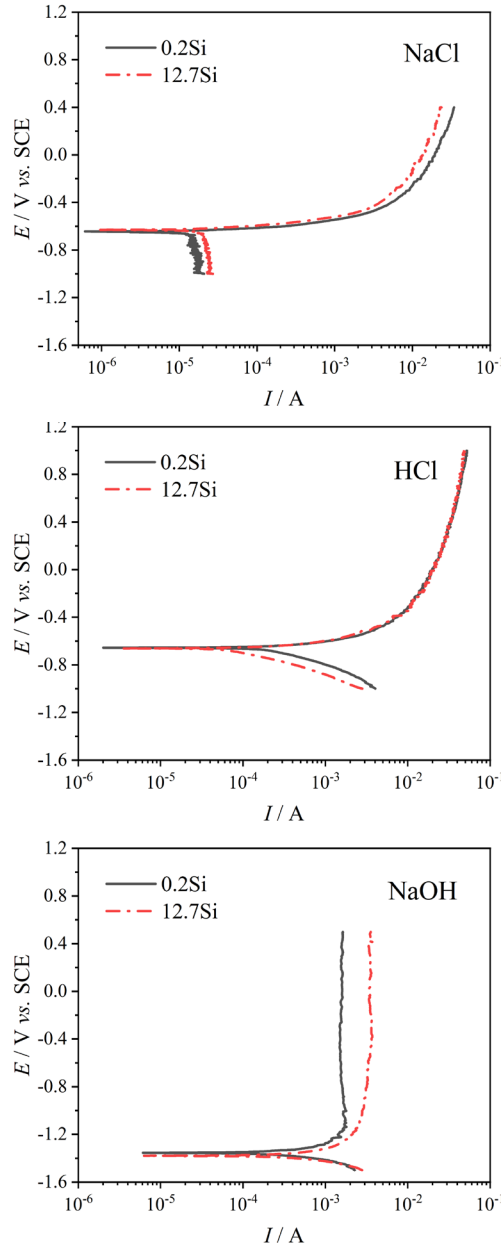

Fig. 4. Tafel plots for trace Si and 12.7Si added Al-Si alloys in: a) 0.2 M NaCl, b) 0.2M HCl, c) 0.2M.

Table 3. Experimental results of potentiodynamic polarization analysis.

Environment	Alloy	Corrosion Current, I_{corr} in µA	Corrosion Potential, E_{corr} in mV	Corrosion Rate in mm year^{-1}
NaCl	0.2Si	25.158	-654.302	1.1667
	12.7Si	15.898	-630.005	0.6911
HCl	0.2Si	248.209	-662.037	10.8817
	12.7Si	152.753	-656.786	6.63116
NaOH	0.2Si	719.301	-1354.797	31.5348
	12.7Si	766.242	-1379.837	33.2633

Optical Micrographic Observation

The optical microstructures of the 0.2Si and 12.7Si added Al-Si alloys are presented in Fig. 5. Polished surfaces with few scratches are shown on the images before corrosion. Post corrosion demolishment of surfaces is clearly visible in the images, where the most deterioration is identified for NaOH solution. More pits and pinholes are seen on the surfaces of trace Si added alloy, but thicker layers are found for 12.7Si added alloy in NaCl and HCl environment. In the alloys, preferential dissolution of active Al particles occurred, and the nobler Si particles were left on the surface. However, a different scenario is observed in case of NaOH solution where the surface is more severely deteriorated for 12.7Si added alloy than 0.2Si added alloy as the attack by OH^- ions cannot be defended by the strengthening effect of Mg_2Si. White spots on the surfaces of the alloys after corrosion correspond to the Al_2O_3 formed after hydrolysis reaction [39]. A yellow green color tone is observed for the surface of each alloy after corrosion, which may

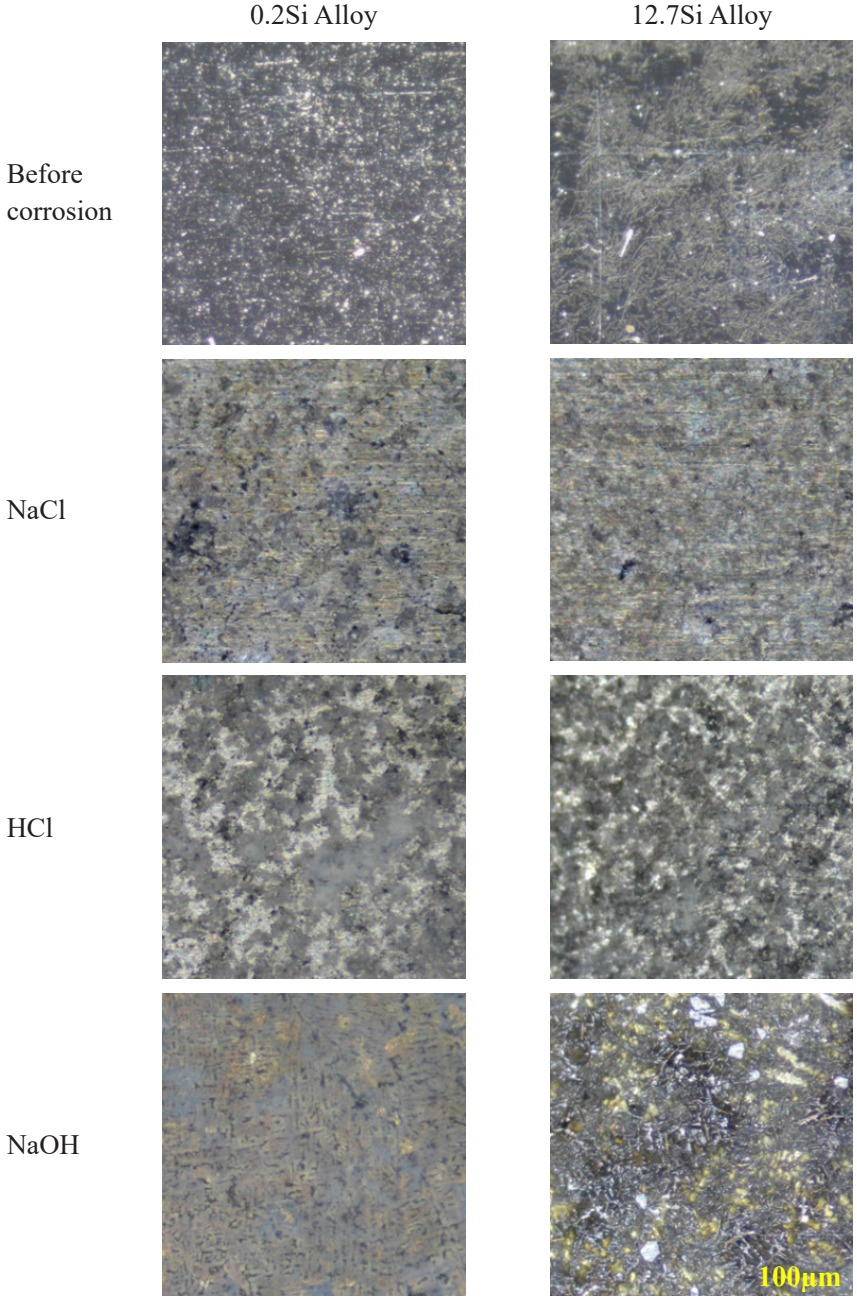

Fig. 5. Optical microstructures of 0.2Si and 12.7Si added Al-Si alloys in 0.2 M NaCl, 0.2 M HCl and 0.2 M NaOH environment.

represent the SiO_2 layer formed [49]. Again, a whitish tone is also observed which may represent the MgO layer formed [50]. The least destruction of the surface seems to have occurred for NaCl environment. Accumulation of Si particles is more visible on the surface of 12.7 Si added alloy in case of NaOH environment, which refers that only silicon has survived the disastrous corrosive effect of OH^- ions, and other elements which could not survive the corrosion attack are dissolved.

SEM and EDX Observation

The SEM images of tested alloys in different environments are shown in Fig. 6. More degraded surfaces are observed for 0.2Si alloy in NaCl and HCl environments. More uniform and stable corrosion occurs on the surfaces of the eutectic alloy in these two environments. However, more scattered, and rapid corrosion is visible for the eutectic alloy in NaOH environment unlike the other two solutions. Polished marks are visible in case of NaCl solution as environment, indicating the least corrosion among all environments, which lies with our previous observation. The protective oxide layers are comparatively more tightly bound with the surface in alloys after corrosion in NaCl environment than in other environments. For NaOH solution, most destruction of surfaces as more cracks and pinholes can be detected. Needle like primary Si particles are visible on the surface of 12.7Si added alloy in NaOH environment, which depict that the surface is severely corroded remaining only the Si particles.

The wt. % elements composition of the surfaces of the alloys is presented in Table 4. It is visibly noticed that the percentage of Al is lowest in NaOH environment,

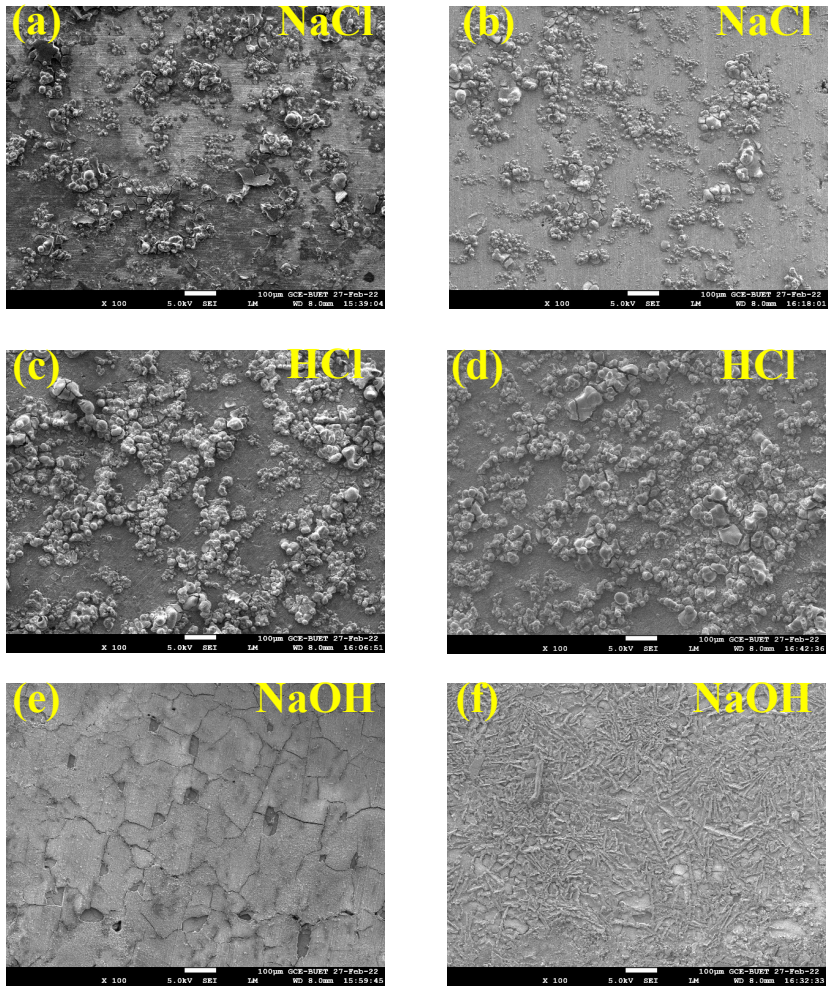

Fig. 6. SEM images for 0.2Si (a, c, e) and 12.7Si (b, d, f) added alloys after electrochemical corrosion in 0.2 M NaCl (a, b); 0.2 M HCl (c, d) and in 0.2 M NaOH (e, f) environment.

Table 4. The composition in wt. %. of the surfaces from the EDX analysis.

Environment	Alloy	Content, wt. %							
		O	Al	Si	Mg	Cl	Fe	Cu	Na
NaCl	0.2Si	27.46	68.38	0.51	0.67	0.73	0.69	1.46	0.10
	12.7Si	32.85	46.78	16.43	0.54	2.08	0.08	1.24	-
HCl	0.2Si	53.17	41.82	0.36	0.22	2.25	1.05	1.13	-
	12.7Si	43.77	34.82	17.66	0.70	1.13	0.6	1.32	-
NaOH	0.2Si	62.55	26.42	0.98	4.31	0.22	-	3.13	2.39
	12.7Si	33.74	10.69	44.53	3.45	0.55	0.73	5.04	1.27

followed by HCl and NaCl for both samples. Again, the percentage of Si is maximum on the surface of the alloy under NaOH environment and then in HCl and NaCl solution in decreasing order, since other elements are dissolved at a greater rate in the most corrosive environment, which NaOH and then HCl according to the results from EIS and potentiodynamic polarization analysis.

CONCLUSIONS

This study researched the corrosion behavior of Al-Si automotive alloy at eutectic level under acid, base, and salt environments and the following conclusions can be drawn:

Corrosion is most destructive if the alloys are immersed in NaOH solution, and least destructive environment is NaCl solution, as OH^- ions attack the surfaces more violently than Cl^- ions, and the Cl^- ions act more disastrous in lower pH; Not only the EIS and potentiodynamic polarization analysis shows this result but also the optical micrographs SEM images support this order of environment for corrosion rate: NaOH > HCl > NaCl; The addition of Si enhances the corrosion performance in NaCl and HCl solution, while NaOH behaving in the opposite way. The corrosion performance gets even deteriorated in higher Si added alloy immersed in NaOH solution; Oxides like SiO_2 and MgO are formed as protective layers in every alloy after corrosion, which can be detected by yellow green tone of the surfaces in optical micrographs. The tone seems deeper in higher Si added alloy in every environment. The coating is thickest in NaOH solution, and thinnest in NaCl solution; The EDX analysis shows lowest concentration of aluminium for the alloy under NaOH and the highest concentration under NaCl. Again, the percentage of Si is maximum in NaOH medium and minimum in NaCl medium, which show that other elements are dissolved at a greater rate in NaOH solution.

Acknowledgements

This study was supported by the ME Dept. of Bangladesh University of Engineering and Technology, Dhaka. The authors thank the Department of Chemistry for the laboratory facilities.

REFERENCES

1. R. Chandel, N. Sharma, S.A. Bansal, A review on recent developments of aluminum-based hybrid composites for automotive applications, Emergent Mater., 4, 5, 2021, 1243-1257.
2. C.S. Ho, M.K. Mohd Nor, An Experimental Investigation on the Deformation Behaviour of Recycled Aluminium Alloy AA6061 Undergoing Finite Strain Deformation, Met. Mater. Int., 27, 12, 2021, 4967-4983.
3. G. Singh, S.L.I. Chan, N. Sharma, Parametric study on the dry sliding wear behaviour of AA6082-T6/TiB2 in situ composites using response surface methodology, J. Brazilian Soc. Mech. Sci. Eng., 40, 6, 2018, 310.
4. R. Rosliza, W.B. Wan Nik, HB Senin, The effect of inhibitor on the corrosion of aluminum alloys in acidic solutions, Mater. Chem. Phys., 107, 2-3, 2008, 281-288.
5. A.A. Mazhar, S.T. Arab, E.A. Noor, The role of chloride ions and pH in the corrosion and pitting of Al-Si alloys, J. Appl. Electrochem., 31, 10, 2001, 1131-1140.
6. J.R. Davis, Corrosion of Aluminum and Aluminum

Alloys, ASM International; USA, 1999.
7. Z. Pilić, I. Martinović, A Comparative Study on the Electrochemical Behaviour of Aluminium and 8090 Al- Li-Cu-Mg Alloy in Acid Rain Solution, Int. J. Electrochem. Sci., 12, 5, 2017, 3576-3588.
8. S. Bedekar, I. Vishwas, D. Priya, Detection of Corrosion using Impedance Spectroscopy, Ferroelectr. Lett. Sect., 35, 1-2, 2008, 7-16.
9. J.H. Perry, Chem. Engineers' Handbook, 3rd edition. New York: McGraw-Hill, USA, 1950.
10. G. Sugiyama, A. Maeda, K. Nagai, Oxidation Degradation and Acid Generation in Diesel Fuel Containing 5% FAME, JSAE/SAE International Fuels & Lubricants Meeting, Kyoto, Japan, 2007.
11. T. Ogawa, S. Kajiya, S. Kosaka, I. Tajima, M. Yamamoto, M. Okada, Analysis of Oxidative Deterioration of Biodiesel Fuel, SAE Int, J, Fuels Lubr., 1, 1, 2009, 1571-1583.
12. T. Omori, A. Tanaka, K. Yamada, S. Bunne, Biodiesel deposit formation mechanism and improvement of Fuel Injection Equipment (FIE), SAE International Powertrains, Fuels and Lubricants Meeting, USA, 2011.
13. S. Herbstman, K. Virk, Use of Dispersants/ Detergents in Diesel Injector Keep Clean and Clean Up Studies, SAE Technical Paperm, USA, 1991.
14. D.M. Thompson, S.R. Nattrass, Full Mid-IR Spectral Characterisation of Lubricant in the Ring Pack of a Running Diesel Engine by Time-Resolved FTIR Spectrometry, Journal of Fuels and Lubr., 105, 4, 1996, 1606-1615.
15. S.A. Lewis, J. Storey, C.S. Sluder, K. Cho, R. Connatser, T. Barone, Carbonyl Formation during High Efficiency Clean Combustion of FACE Fuels, SAE Int J Fuels Lubr, 3, 2, 2010, 2010-01-2212.
16. D. Sullivan, The Role of Merox Process in the Era of Ultra Low Sulfurtransportation Fuels, In: EMEA Catalyst Technology Conference. 2004.
17. K. Owen, T. Coley, Automotive Fuels Reference Book, 2nd edition. United States.
18. J. Barker, S. Cook, P. Richards, Sodium contamination of diesel fuel, its interaction with fuel additives and the resultant effects on filter plugging and injector fouling, SAE Int J Fuels Lubr, 6, 3, 2013, 2013-01-2687.
19. M.D. Cardenas Almena, O. Lucio Esperilla, F. Martin Manzanero, Y. Murillo Duarte, L.C. Quintero Toscano, G. Wolff, Internal diesel injector deposits: sodium carboxylates of C12 succinic acids and C16 and C18 fatty acids, SAE International Powertrains, Fuels & Lubricants Meeting, USA, 2012.
20. A.A. Khan, M.R. Shoummo, M.S. Kaiser, Surface Quality of Fe , Ni , and Cr added Hyper-eutectic Al-Si Automotive Alloys under Up-milling and Down-milling Operation, J. Mechanical Eng. Sci. Technol., 6, 1, 2022, 9-22.
21. H. Torabian, J.P. Pathak, S.N. Tiwari, Wear characteristics of Al-Si alloys, Wear, 172, 1, 1994, 49-58.
22. M. Al Nur, A.A. Khan, S. Dev Sharma, M.S. Kaiser, Electrochemical corrosion performance of Si-doped Al-based automotive alloy in 0.1 M NaCl solution, J. Electrochem. Sci. Eng., 12, 3, 2022, 565-576.
23. J.L. Murray, A.J. McAlister, The Al-Si (Aluminum-Silicon) system, Bull Alloy Phase Diagrams, 5, 1, 1984, 74-84.
24. F. Mansfeld, M.W. Kendig, Technical Note: Impedance Spectroscopy as Quality Control and Corrosion Test for Anodized Al Alloys, CORROSION, 41, 8, 1985, 490-492.
25. C.L.C. Ellis, E. Smith, H. Javaid, G. Berns, D. Venkataraman, Ion Migration in Hybrid Perovskites, In: Perovskite Photovoltaics, Elsevier, 2018. 163-196.
26. R. Keshavamurthy, C.S. Ramesh, G.S. Pradeep Kumar, V. Tambrallimath, Experimental investigation of tribocorrosion, In: Tribocorrosion, Elsevier, 2021, 17-42.
27. J.T. Staley, D.J. Lege, Advances in aluminium alloy products for structural applications in transportation, J. Phys. IV France, 03, C7, 1993, 179-190.
28. S. Anand, T.S. Srivatsan, Y. Wu, E.J. Lavernia, Processing, microstructure and fracture behaviour of a spray atomized and deposited aluminium-silicon alloy, J. Mater. Sci., 32, 11, 1997, 2835-2848.
29. A.A. Razin, D.S. Ahammed, M. Al Nur, M.S. Kaiser, Role of Si on machined surfaces of Al-based automotive alloys under varying machining parameters, J. Mech. Energy Eng., 6, 1, 2022, 43-52.
30. P.D. Reena Kumari, J. Nayak, A. Nityananda Shetty, Corrosion behavior of 6061/Al-15 vol. pct. SiC(p) composite and the base alloy in sodium hydroxide solution, Arab J. Chem., 9, 2016, S1144-S1154.
31. X. Li, S. Deng, H. Fu, G. Mu, Inhibition effect of

6-benzylaminopurine on the corrosion of cold rolled steel in H2SO4 solution, Corros. Sci., 51, 3, 2009, 620-634.
32. J. Bessone, C. Mayer, K. Jüttner, W.J. Lorenz, AC-impedance measurements on aluminium barrier type oxide films, Electrochim Acta, 28, 2, 1983, 171-175.
33. H.S. Magar, R.Y.A. Hassan, A. Mulchandani, Electrochemical Impedance Spectroscopy (EIS): Principles, Construction, and Biosensing Applications, Sensors, 21, 19, 2021, 1-21.
34. W.A.W.E. Amira, A.A. Rahim, H. Osman, K. Awang, P.B. Raja, Corrosion inhibition of mild steel in 1 M HCl solution by Xylopia ferruginea leaves from different extract and partitions, Int. J. Electrochem. Sci., 6, 7, 2011, 2998-3016.
35. J. Cruz, T. Pandiyan, E. García-Ochoa, A new inhibitor for mild carbon steel: Electrochemical and DFT studies, J. Electroanal. Chem., 583, 1, 2005, 8-16.
36. S. Choudhary, A. Garg, K. Mondal, Relation between open circuit potential and polarization resistance with rust and corrosion monitoring of mild steel, J. Mater. Eng. Perform., 25, 7, 2016, 2969-2976.
37. A. Hossain, M.A. Gafur, F. Gulshan, A.S.W. Kurny, The effects of 2wt % Cu addition on the corrosion behavior of heat treated Al-6Si-0.5Mg-2Ni alloy, International Journal of Materials and Metallurgical Engineering, 8, 7, 2014, 719-723.
38. A.S. Fouda, F.S. Mohamed, M.W. El-Sherbeni, Corrosion Inhibition of Aluminum-Silicon Alloy in Hydrochloric Acid Solutions Using Carbamidic Thioanhydride Derivatives, J Bio- Tribo-Corros., 2, 2, 2016, 11.
39. J-H. Yoo, K-S. Yun, R.S. Kalubarme, C-N. Park, C-J. Park, Hydrogen generation using the corrosion of Al-Sn and Al-Si alloys in an alkaline solution, Met. Mater. Int., 20, 4, 2014, 619-627.
40. T. Zheng, L. Wang, J. Liu, J. Wang, G. Jia, The corrosion inhibition effect of sodium silicate and Triton X-100 on 2024-T3 aluminum alloy in NaOH medium: Experimental and theoretical research, Colloids Surfaces A Physicochem. Eng. Asp., 610, 2021, 125723.
41. R. Parsons, Atlas of electrochemical equilibria in aqueous solutions, J. Electroanal Chem. Interfacial Electrochem, 13, 4, 1967, 331-342.
42. M. Lashgari, A.M. Malek, Fundamental studies of aluminum corrosion in acidic and basic environments: Theoretical predictions and experimental observations, Electrochim. Acta, 55, 18, 2010, 5253-5257.
43. A.A. Khan, M.S. Kaiser, Electrochemical corrosion performance of eutectic Al-Si automotive alloy in 0.1 M and 0.2 M NaCl solution, IOP Conf. Ser. Mater. Sci. Eng., 1248, 1, 2022, 012031.
44. R. Escalera-Lozano, M.I. Pech-Canul, M.A. Pech-Canul, M. Montoya-Davila, A. Uribe-Salas, The role of Mg2Si in the corrosion behavior of Al-Si-Mg alloys for pressureless infiltration, Open Corros. J., 3, 1, 2010, 73-79.
45. W.R. Osório, P.R. Goulart, A. Garcia, Effect of silicon content on microstructure and electrochemical behavior of hypoeutectic Al-Si alloys, Mater Lett., 62, 3, 2008, 365-369.
46. N.L. Sukiman, X. Zhou, N. Birbilis, A.E. Hughes, J.M.C. Mol, S.J. Garcia Espallargas, X. Zhou, G.E. Thompson, Durability and Corrosion of Aluminium and Its Alloys: Overview, Property Space, Techniques and Developments, In: Aluminium Alloys - New Trends in Fabrication and Applications. InTech, London, UK, 2012.
47. M. Abdallah, E.M. Kamar, S. Eid, A.Y. El-Etre, Animal glue as green inhibitor for corrosion of aluminum and aluminum-silicon alloys in sodium hydroxide solutions, J Mol Liq., 220, 2016, 755-761.
48. R.I. Revilla, J. Liang, S. Godet, I. De Graeve, Local Corrosion Behavior of Additive Manufactured AlSiMg Alloy Assessed by SEM and SKPFM, J. Electrochem Soc., 164, 2, 2017, C27-C35.
49. R.C. Jaeger, Introduction to Microelectronic Fabrication, 2nd edition. Prentice Hall, NewJersey, USA, 2001.
50. PubChem Compound Summary for CID 14792, Magnesium oxide, National Library of Medicin, Bethesda, USA, 2022.